

Exploring the Interfacial Hydrogen Transfer between Pt and the Siliceous Framework and Its Promotional Effect on the Isotope Catalytic Exchange

Hongbing Wang, Yifei Yang,* Yida Zhou, Jun Chen, Dongping Wang, Wei Cui, Linsen Zhou, Shutao Xu,* and Yunxi Yao*



Cite This: *ACS Appl. Mater. Interfaces* 2024, 16, 31126–31136



Read Online

ACCESS |



Metrics & More

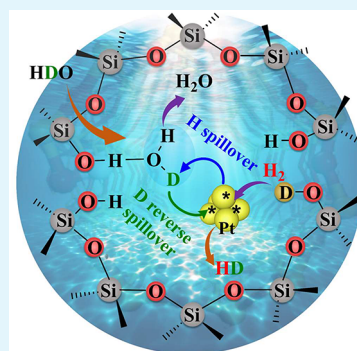


Article Recommendations



Supporting Information

ABSTRACT: Interfacial hydrogen transfer between metal particles and catalyst supports is a ubiquitous phenomenon in heterogeneous catalysis, and this occurrence on reducible supports has been established, yet controversies remain about how hydrogen transfer can take place on nonreducible supports, such as silica. Herein, highly dispersed Pt clusters supported on a series of porous silica materials with zeolitic or/and amorphous frameworks were prepared to interrogate the nature of hydrogen transfer and its promotional effect on H₂–HDO isotope catalytic exchange. The formation of zeolitic frameworks upon these porous silica supports by hydrothermal crystallization greatly promotes the interfacial hydrogen bidirectional migration between metal clusters and supports. Benefiting from this transfer effect, the isotope exchange rate is enhanced by 10 times compared to that on the amorphous counterpart (e.g., Pt/SBA-15). In situ spectroscopic and theoretical studies suggest that the defective silanols formed within the zeolite framework serve as the reactive sites to bind HDO or H₂O by hydrogen bonds. Under the electrostatic attraction interaction, the D of hydrogen-bonded HDO scrambles to the Pt site and the dissociated H on Pt simultaneously spills back to the electronegative oxygen atom of adsorbed water to attain H–D isotope exchange with an energy barrier of 0.43 eV. The reverse spillover D on Pt combines with the other H on Pt to form HD in the effluent. We anticipate that these findings are able to improve our understanding of hydrogen transfer between metal and silica supports and favor the catalyst design for the hydrogen-involving reaction.



KEYWORDS: hydrogen transfer, isotope exchange, zeolite framework, spillover, silanol nest

1. INTRODUCTION

Ordered micro/meso-porous silica materials with abundant surface chemistry, high surface-to-volume ratios, and advantageous morphological and physicochemical properties have attracted considerable attentions over the last few decades for their uses in heterogeneous catalysis.^{1–3} The robust skeletal structures and well-developed microchannels enable these materials to be unique with the desirable function that encapsulates metal clusters into cavities for the hydrogen-involving catalytic processes, such as the deuterium substitution of ethylbenzene on Pt@NaA/H-USY,⁴ the selective hydrogenation of quinolines on Pt@HA,⁵ and the cyclohexane dehydrogenation on Pt-encapsulated aluminosilicates.⁶ Upon these bifunctional catalysts, the superior catalytic reactivities are always related to the enhanced hydrogen transfer between metal and supports, because these support materials are inert for hydrogen activation, and the only adsorbed hydrogen on metal migrates to the reactive sites contained within supports to catalyze the subsequent reaction. This interfacial transfer usually requires an energetically efficient pathway to deliver the active hydrogen species (e.g., hydrogen radical (H•), proton (H⁺), or hydride (H⁻)) over the dual sites.

Hydrogen transfer, referred as to hydrogen spillover, primarily occurs at the interface of metal particles and reducible M_xO_y supports,⁷ during which the dissociated hydrogen transforms into a proton–electron pair and the isolated proton is captured by the lattice O²⁻ anion under electrostatic attraction, causing the partial reduction of Mⁿ⁺ to M⁽ⁿ⁻¹⁾⁺ cation by an electron.⁸ For example, hydrogen uptake on Pt/MoO₃ led to the formation of H_xMoO₃ species because of the diffusion of spillover hydrogen into bulk.⁹ For the nonreducible supports (e.g., SiO₂, MgO, and Al₂O₃), the hydrogen spillover between metal and support is believed to be energetically improbable because the wide band gap of these materials enables the electron hopping to valence band and the migration of cation–electron pairs on supports to be impracticable.^{10,11} To boost the metal-catalyzed hydrogen-

Received: March 10, 2024

Revised: May 22, 2024

Accepted: May 23, 2024

Published: June 5, 2024



involving reaction on these nonreducible supports, a series of strategies were developed to improve hydrogen spillover, such as modifying the organic species on the silica surface^{12,13} and hydrothermally treating the siliceous framework to zeolitize by Al incorporation.^{14,15} For hydrogen migration upon the aluminosilicate solids, theoretical studies demonstrated that the local structural distortion of Al-incorporated units ($-\text{Si}-\text{OH}-\text{Al}-$) is an essential prerequisite for hydrogen transfer in the form of proton and the presence of a defective Lewis site assures the consecutive movement of proton–electron pairs.¹⁶ However, for the pure silica zeolites (e.g., Silicalite-1), the lack of structural distortion and Coulombic interaction imposed by Al substitution enables hydrogen transfer between metal and supports to remain elusive. Nonetheless, these materials supported catalysts are reported to be more reactive for alkane dehydrogenation than their amorphous counterparts,^{17–20} and the promotional effect has not been unambiguously addressed, especially in the hydrogen transfer processes. Understanding the mechanistic basis of hydrogen transfer is indispensable for screening the suitable catalysts for hydrogen-involving processes, such as hydrogen–water isotope exchange (e.g., $\text{H}_2(\text{g}) + \text{HDO}(\text{l}) = \text{HD}(\text{g}) + \text{H}_2\text{O}(\text{l})$), a promising reaction catalyzed by metallic Pt for the deuterium extraction from seawater and the detritiation of nuclear wastewater.^{21–23} Due to the great difficulty of water activation on the Pt surface,²⁴ this reaction requires an effective route to transport the active hydrogen species over the spatially separate sites.

Herein, a series of microporous/mesoporous silica materials (e.g., Silicalite-1 and SBA-15) with zeolitic or/and amorphous frameworks were used to support the highly dispersed Pt clusters for exploring the interfacial hydrogen transfer between metal and supports and its catalytic function during H_2 –HDO isotope exchange. It is found that the formation of zeolitic frameworks within these porous solids is indispensable for the interfacial hydrogen migration, which could improve the isotope exchange rate by 10 times as compared to that on traditional Pt/SBA-15. In situ spectroscopic and theoretical studies suggest that the defective silanols formed within the zeolite framework function as the reactive sites, which could stabilize HDO or H_2O by hydrogen bond interactions. Subsequently, the D of hydrogen-bonded HDO and the adsorbed H on Pt undergo a simultaneous and bidirectional migration in the positively charged form to attain H–D isotope exchange with an energy barrier as low as 0.43 eV. Ultimately, the reverse split-over D on Pt combines with the other H to desorb, contributing to the observed HD product.

2. EXPERIMENTAL AND SIMULATION METHOD

2.1. Preparation of the Hydrophobic Pt Catalyst. The highly crystalline Silicalite-1 zeolite was hydrothermally synthesized by following the method reported in the literature.²⁵ Typically, 8.12 g of tetrapropylammonium hydroxide solution (TPAOH, 25 wt %, Maclin), 8.24 g of tetraethyl orthosilicate (TEOS, 99.9%, Maclin), and 20.1 g of deionized water were mixed and agitated at ambient temperature for 6 h. The resultant mixtures were transferred to Teflon-lined autoclaves and heated in an electric oven at 453 K for 72 h under static conditions. The products were recovered by filtration and thoroughly washed with deionized water, dried at 333 K for 10 h, and calcined under an air flow at 823 K for 6 h.

The zeolitization of amorphous SBA-15 samples was performed by hydrothermally treating the commercially available SBA-15 (99.9%, surface area: 450 m^2/g , XFNANO) with TPAOH as a structure-directing agent. The molar composition was 1 SBA-15:0.14 NaOH:0.025 TPAOH:8.5 H_2O . Powder SBA-15, TPAOH, NaOH,

and deionized water were initially mixed and stirred for 12 h at room temperature. Then, the mixtures were transferred into autoclaves and treated at 423 K for a certain number of hours. The resultant products were collected by centrifuging, rinsing with deionized water, drying at 353 K for 10 h, and calcining at 823 K for 6 h in flowing air. The as-synthesized samples were denominated as Sil-R- x , where x denotes the hour of hydrothermal treatment.

Hydrophobic Pt catalysts were prepared by incipient wetness impregnation and postsilylation. Impregnation was performed by adding the desirable supports (e.g., Silicalite-1, SBA-15, and Sil-R- x) into the diluting $\text{Pt}(\text{NH}_3)_4(\text{NO}_3)_2$ (Aladdin, Pt \geq 50%) solution to maintain the nominal Pt loading of 1 wt %. These mixtures subsequently were dried at 353 K for 6 h, followed by heating at the rate of 2 K min^{-1} in 20% H_2 –Ar (100 mL min^{-1}) to 573 K and then holding at 573 K for 5 h. The hydrophobic modification was carried out by dispersing the desiccative catalysts into ethanol containing the desirable amount of hexadecyltrimethoxysilane (HDTMS, Aladdin, 95%) under vigorous stirring and introducing HNO_3 (0.1 $\text{mol}\cdot\text{L}^{-1}$) to catalyze the hydrolysis of HDTMS. After filtration, the catalyst powders were washed with ethanol, dried overnight at 353 K, and labeled as 1Pt/Silicalite-1, 1Pt/SBA-15, and 1Pt/Sil-R- x .

2.2. Characterization of Hydrophobic Pt Catalysts. X-ray diffraction (XRD) analysis was performed on a Bruker D8 Discover diffractometer with monochromatized $\text{Cu K}\alpha$ radiation, and the patterns were collected in the range at $2\theta = 10\text{--}70^\circ$ with a resolution of 0.025° . Nitrogen physisorption was measured by using an ASAP2460 Micromeritics instrument at the temperature of liquid nitrogen to acquire the textural parameters such as the specific surface area (S_{BET}), pore volume (V_t), and pore size distribution. Prior to the measurements, all samples were degassed at 573 K for 6 h. Solid-state magic-angle-spinning nuclear magnetic resonance (MAS NMR) measurements were conducted on a Bruker Avance NEO 500 spectrometer operating at a frequency of 99.36 MHz for the ^{29}Si nucleus. ^{29}Si MAS NMR spectra with high-power proton decoupling were recorded by using a $\pi/4$ pulse of 3.9 μs and a recycle delay of 60 s on a 4 mm MAS probe with a spinning rate of 10 kHz. For ^1H – ^{29}Si cross-polarization (CP) MAS NMR measurements, the Hartmann–Hahn condition was achieved with a contact time of 3 ms and a recycle delay of 2 s. The morphological observation of Pt catalysts by scanning transmission electron microscopy (STEM) was carried out on an FEI Talos F200X instrument operated at a voltage of 200 kV. The catalyst powders were ultrasonically dispersed in ethanol and deposited on a copper grid. The average particle size is measured by randomly extracting 100 monodispersed Pt particles from the different regions to calculate their weighted average.

CO or pyridine adsorption on the as-synthesized sample was measured on a Nicolet iSS0 Fourier transform infrared (FT-IR) spectrometer by using an MCT detector. The customized reactor cell for transmission analysis was sealed with ZnSe windows and connected to a pump station, which could be operated at the temperature range of 298–673 K and the evacuation to less than 1×10^{-5} Pa. Catalyst powders were pelleted into a wafer and reduced at 573 K under flowing H_2 for 1 h. After evacuation to $\sim 10^{-4}$ Pa, a trace amount of purified CO (99.999%, Messer) or pyridine (99.5%, Macklin) vapor was introduced into the cell at 298 or 353 K via using a precision valve for adsorption, respectively. The resultant FT-IR spectra were collected at a resolution of 4 cm^{-1} and 32 scans per spectrum under absorbance mode. The quantitative analysis of Brønsted (C_B) and Lewis acid (C_L) concentrations upon these samples was performed by integrating the absorption bands at 1545 and 1455 cm^{-1} in the pyridine-adsorbed spectra, respectively, based on the previously reported method.²⁶

$$C_B = 1.88 \times I_B \times \frac{R^2}{W} \quad (1)$$

$$C_L = 1.42 \times I_L \times \frac{R^2}{W} \quad (2)$$

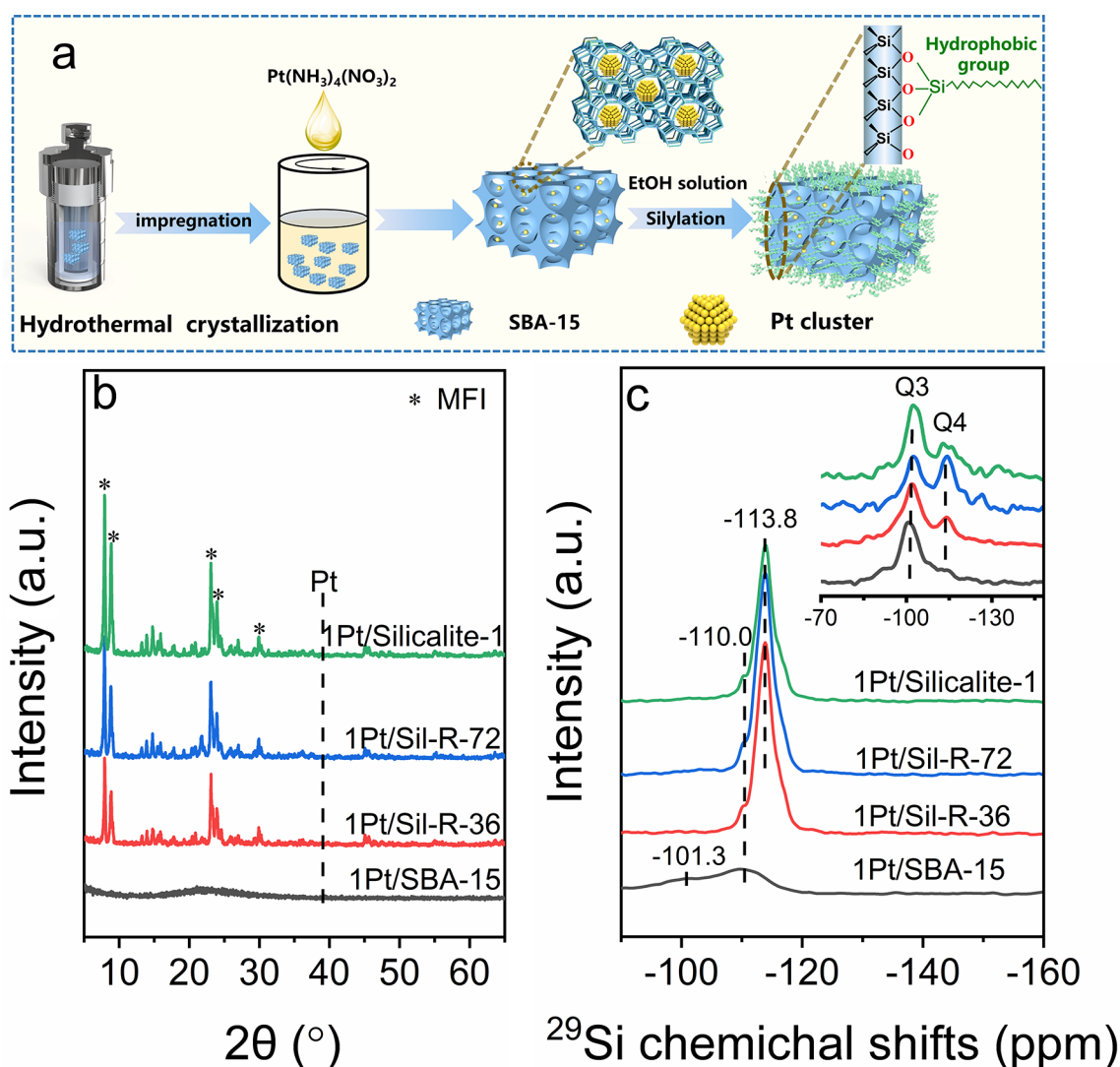


Figure 1. (a) Schematic of the preparation procedure of hydrophobic Pt catalysts. (b) XRD and (c) ^{29}Si MAS NMR spectra of as-synthesized Pt catalysts. The inset in panel (c) is the ^{29}Si CP MAS NMR spectra.

where I_B and I_L represent the integrated intensities of pyridine adsorbed on Brønsted and Lewis acid sites, respectively, and R and W denote the radius (cm) and weight (mg) of the catalyst wafer, respectively.

The transient surface reaction (TSR) of D_2 and H_2O on these Pt catalysts was measured by using an online mass spectrometer (MS) to trace the composition of the effluents. Typically, 0.1 g of catalyst powder was placed into a tubular reactor and reduced at 573 K for 1 h with 20% H_2 -Ar (80 mL min^{-1}), followed by purging at 573 K in the flowing Ar (100 mL min^{-1}) for 3 h. After cooling to 353 K, the purified 10% D_2 -10% N_2 -Ar mixture (80 mL min^{-1} , N_2 as internal standard) was fed into the reactor by using MS to trace the signals of H_2 ($m/z = 2$), HD ($m/z = 3$), and D_2 ($m/z = 4$). After reaction, H_2O vapor ($\sim 10 \text{ kPa}$) was introduced into the reactor by injecting H_2O into a vaporization zone with a gastight syringe mounted on an infusion pump and combining with the 10% N_2 -Ar stream (80 mL min^{-1}). The effluent was analyzed by MS to monitor H_2O ($m/z = 18$) and HDO ($m/z = 19$) signals.

In situ FT-IR spectra of D_2 and H_2O adsorption on these Pt catalysts were acquired by using the above-mentioned instrument. Similarly, the catalyst wafer was reduced to 573 K and evacuated to 10^{-4} Pa for the subsequent adsorption. The purified D_2 (99.99%, Messer) and H_2O (or D_2O) (99.99%, Sigma-Aldrich) by a freezing-pumping-thawing trap were introduced into the cell at 353 K by a

leak valve to record the absorbance data at a resolution of 4 cm^{-1} and 32 scans per spectrum.

2.3. Catalytic Performance of Hydrogen Isotope Exchange.

The catalytic performance of hydrogen isotope exchange between hydrogen and water was evaluated on a microcatalytic quartz reactor equipped with a K-type thermocouple that was placed at the center of the packed catalyst bed. The reactant 20 wt % HDO- H_2O was prepared by physically mixing D_2O (99.9 atom % D, Innochem) and deionized H_2O . Catalyst powders were pelleted into discs, crushed, and sieved to acquire 40–60 mesh aggregates for reaction. Before the reactants were fed, these Pt catalysts were reduced at 573 K for 2 h in flowing H_2 . When cooling to the reaction temperature, the liquid deuterated water was injected into the reactor via a syringe mounted on an infusion pump (Longer D1sp 510) to mix with 80% H_2 -Ar and to obtain a constant space velocity of $1.1 \times 10^6 \text{ mL g}_{\text{cat}}^{-1} \text{ h}^{-1}$. The intrinsic reactivities of H_2 -HDO exchange on Pt catalysts were measured under the gas-phase condition by injecting 20% HDO- H_2O into a vaporization zone to maintain a constant space velocity of $5 \times 10^6 \text{ mL g}_{\text{cat}}^{-1} \text{ h}^{-1}$. Before analyzing the product by an online gas chromatograph (GC), the downstream gas lines were connected to two cold traps and then to a desiccant tack to completely remove water. The GC is equipped with a carbon molecular sieve column and a thermal conductivity detector (TCD), which was operated with hydrogen as the carrier gas.

Table 1. Quantitative Analysis of Textural Properties, Acidities, and Activation Energies of Different Pt Catalysts

sample	N ₂ physisorption				pyridine adsorption		E _a (kJ mol ⁻¹)
	S _{BET} (m ² g ⁻¹)	V _t (cm ³ g ⁻¹)	V _m (cm ³ g ⁻¹)	D _p (nm)	C _B (μmol g ⁻¹)	C _L (μmol g ⁻¹)	
1Pt/SBA-15	458.2	1.20	0.03	7.7	0	78.9	49.2 ± 2.0
1Pt/Sil-R-36	388.6	0.11	0.10	1.9, 3.4	2.1	33.8	40.3 ± 2.2
1Pt/Sil-R-72	433.8	0.14	0.10	5.2	5.2	92.4	38.6 ± 2.0
1Pt/Silicalite-1	302.7	0.17	0.12	2.9	4.8	166.7	36.9 ± 1.6

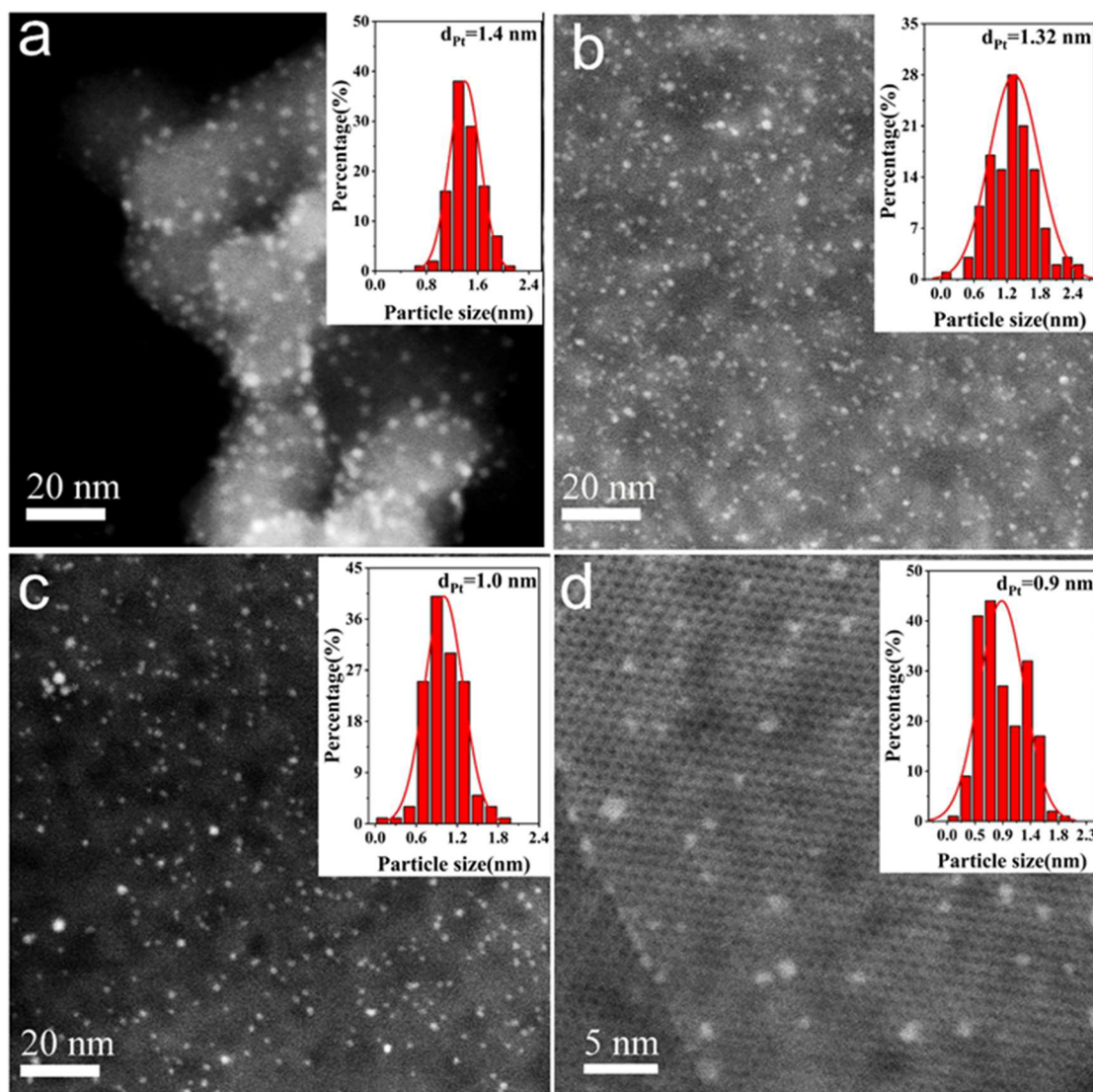


Figure 2. Representative HAADF-STEM micrographs of (a) 1Pt/SBA-15, (b) 1Pt/Sil-R-36, (c) 1Pt/Sil-R-72, and (d) 1Pt/Silicalite-1 with the particle size distribution in the inset.

2.4. DFT Calculations. The periodic density functional theory (DFT) calculations were carried out with the Vienna Ab Initio Simulation Package (VASP) with the projector augmented wave (PAW) method. The effect of van der Waals interactions was described by the DFT-D3 correction, and the exchange functional was treated by using the generalized gradient approximation (GGA) with the Perdew–Burke–Ernzerhof (PBE) functional. The energy cutoff for the plane wave basis expansion was set to 450 eV. Partial occupancies of Kohn–Sham orbitals were treated using the Gaussian smearing method with a width of 0.2 eV. The orthorhombic cell of MFI was used to model the Silicalite-1 zeolite with the bulk cell parameters and the initial ionic positions obtained from the International Zeolite Association database. A crystalline silica (001) surface, extracted from the bulk phase of α -quartz, was constructed

with all dangling bonds saturated by hydrogen atoms to represent SBA-15 based on the reported methods in the literature.^{27,28} The Monkhorst–Pack k -points of $1 \times 1 \times 1$ and $2 \times 2 \times 1$ were used to sample the Brillouin zone of the Silicalite-1 zeolite and SBA-15, respectively. The convergence thresholds for energies and forces were set to 10^{-5} eV and 0.05 eV/Å, respectively.

3. RESULTS AND DISCUSSION

3.1. Structural Characterization of Supported Pt Catalyst. Supported Pt clusters on the series of micro/mesoporous silica solids (Silicalite-1, SBA-15, and Sil-R- x) with the varied framework structures were prepared by incipient wetness impregnation and postsilylation, as described

in Figure 1a. The structural crystallinities of these Pt catalysts were subjected to the characterization of X-ray diffraction (XRD). As illustrated in Figure 1b, the primary diffraction peaks for 1Pt/Silicalite-1 centered at 7.9° , 8.9° , 23.0° , and 23.9° correspond to the (101), (020), (151), and (303) reflections of MFI-type zeolite (PDF#44-0003),²⁹ respectively. During nitrogen physisorption, this microporous zeolite exhibits the typical type-I isotherm (shown in Figure S1) and possesses the specific surface area (S_{BET}) of $302.7 \text{ m}^2 \text{ g}^{-1}$ and micropore volume (V_{m}) of $0.12 \text{ cm}^3 \text{ g}^{-1}$, as summarized in Table 1. For mesoporous SBA-15, the disordered stacking of building blocks leads to the absence of any diffraction signals and the measured sorption isotherm renders the type-IV curve with the hysteresis loop at $P/P_0 = 0.6\text{--}0.9$. The total pore volume (V_{t}) is up to $1.2 \text{ cm}^3 \text{ g}^{-1}$ and primarily stems from the contribution of mesopores. When using SBA-15 as seeds to zeolitize under the hydrothermal conditions, the amorphous silica framework partially dissolves in the basic agents and experiences the structural assembly with the assistance of structure-directing agent to form a zeolitic framework with the diffraction features of MFI for the 1Pt/Sil-R-36 and 1Pt/Sil-R-72 samples. The zeolitization treatment enables the mesoporous characteristic of SBA-15 to be faded because of the dissolution and collapse of the silica framework. The measured micropore volumes (V_{m}) in Table 1 for these two samples are both up to $0.1 \text{ cm}^3 \text{ g}^{-1}$, approaching the value of the 1Pt/Silicalite-1 sample. Additionally, it is worth noting that Pt diffraction signals are absent upon all of these Pt catalysts, which suggests that Pt species are highly dispersed on these high-surface-area porous solids. Further, the architectural features of these siliceous supports were characterized by ^{29}Si magic-angle-spinning nuclear magnetic resonance (MAS NMR) with the high power proton decoupling. The resonance spectra in Figure 1c for the 1Pt/Silicalite-1 and 1Pt/Sil-R-*x* samples with zeolitic frameworks predominantly center at -113.8 ppm , attributing to the typical $\text{Si}(\text{OSi})_4(\text{Q4})$ unit.³⁰ Additionally, a satellite peak emerged at -110.0 ppm is also related to the Q4 coordination with the crystallographically distinct T-sites.³¹ By the cross-polarization of $^1\text{H}\text{--}^{29}\text{Si}$, the polarized Q3 signals are observed for these samples in the inset, which implies the presence of abundant silanols within these zeolite frameworks and the proximity to Si sites with Q4 and Q3 coordination. In contrast, the resonance for 1Pt/SBA-15 exhibits a broad peak with the characteristic signals at -110.0 and -101.3 ppm , ascribing to the $\text{Si}(\text{OSi})_4(\text{Q4})$ and $\text{Si}(\text{OSi})_3\text{OH}(\text{Q3})$ coordination,^{32,33} respectively. Correspondingly, only the polarized Q3 signal in the CP MAS NMR spectrum is monitored, which suggests that the dominant silanols on SBA-15 have proximity to the Q3-type Si.

The morphological features of Pt catalysts were observed by scanning transmission electron microscopy (STEM). Figures 2a–2d show the representative STEM imaging of as-synthesized Pt catalysts. Under the mode of high-angle annular dark field (HAADF), the high *z*-contrast enables Pt clusters to emerge in the form of white spots, which are uniformly distributed on these porous silica frameworks with the ensemble-averaged particle size of 1.2 nm. Although the surface area and pore volume of microporous Silicalite-1 are much less than those of mesoporous SBA-15, the supported Pt clusters possess the similar particle size at the identical metal loading, which suggests the enriched channels of these porous solids are efficient to sterically confine Pt clusters. The high-resolution observation of Silicalite-1 enables the microporous

zeolite cage to be clearly discerned in the magnification of 2.5 Mx. On this basis, the surface chemical states of these fine Pt clusters were interrogated by in situ CO adsorbed Fourier transform infrared (FT-IR). As shown in Figure 3a, exposure

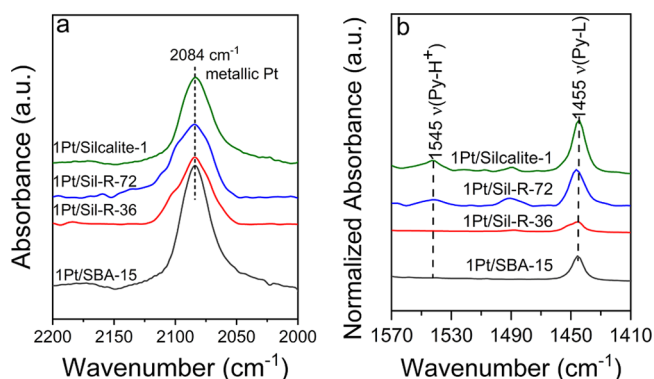


Figure 3. In situ (a) CO and (b) pyridine adsorbed FT-IR spectra of as-synthesized Pt catalysts, which were pretreated in the flowing H_2 at 573 K. The normalization of pyridine adsorbed spectra was performed by using the overtone lattice bands at 2000 and 1875 cm^{-1} as the standard.

of 1 Pa of CO to these prerduced Pt catalysts causes the characteristic C–O stretching vibration to emerge at 2084 cm^{-1} . This vibrational wavenumber is associated with the linearly adsorbed CO on metallic Pt clusters,³⁴ which is also consistent with the surface valence state of Pt catalysts characterized by X-ray photoelectron spectroscopy (XPS) in Figure S2. Additionally, the surface acidities of these siliceous materials are pivotal to mediate the hydrogen transfer, because the previous studies found that the energetically favorable hydrogen transfer on zeolitic aluminosilicate proceeds in the form of proton hopping.³⁵ Pyridine adsorption by in situ FT-IR was used to probe the surface acidities of as-synthesized Pt catalysts. As demonstrated in Figure 3b, the absorption bands at 1545 and 1455 cm^{-1} are ascribed to pyridine adsorbed on the Brønsted and Lewis acid sites,^{36–38} respectively. The quantitative concentrations of Brønsted acid (BA) for these siliceous solids in Table 1, estimated by integrating the absorption band at 1545 cm^{-1} as discussed in the experimental section, are approximately $0\text{--}5 \mu\text{mol}\cdot\text{g}^{-1}$, which is significantly lower than the reported value of $\sim 220 \mu\text{mol}\cdot\text{g}^{-1}$ for the Al-incorporated ZSM-5 zeolite at Si/Al = 30 and could be ignorable.³⁹ Collectively, these results confirm that the highly dispersed Pt clusters on the porous siliceous framework always remain in their metallic state and the as-synthesized Pt catalysts are BA-free ones for the catalytic exchange.

3.2. Catalytic Performances of Pt Catalysts during Hydrogen Isotope Exchange. Hydrogen water isotope catalytic exchange was used as a probe reaction to evaluate the catalytic performance of as-synthesized Pt catalysts. To measure the catalytic data, 80% $\text{H}_2\text{--Ar}$ and liquid 20% HDO– H_2O were fed into a fixed bed reactor to contact with Pt catalysts. These hydrophobic catalysts with a measured contact angle of $143 \pm 3^\circ$ in Figure S3 by silylation modification are effective to surmount the flooding of metal sites by liquid water and enable the active sites to be highly accessible for H_2 . The space velocities were tuned by interpellet dilution with their support materials and estimated by the total stream of $\text{H}_2\text{--Ar}$ and saturated water vapor. The used Silicalite-1 and SBA-15 supports were verified to be inert

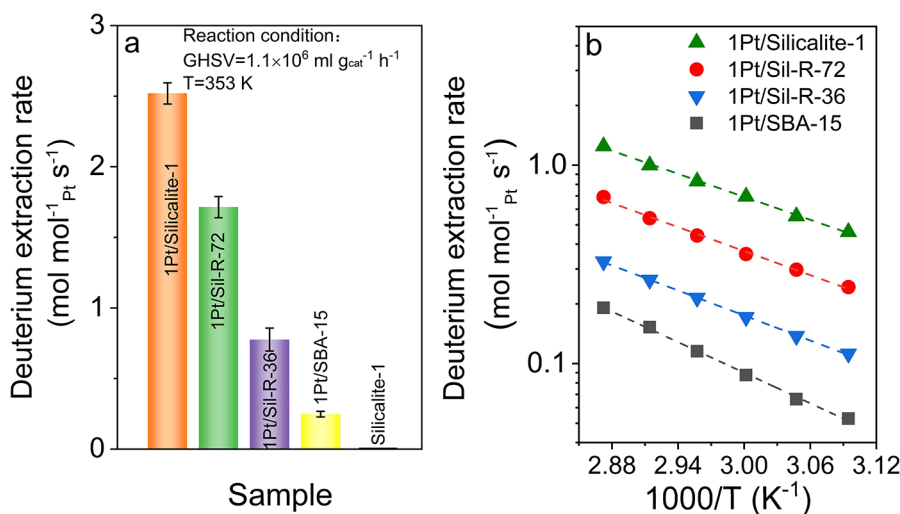


Figure 4. (a) The comparison of deuterium extraction rate of H₂–HDO isotope exchange upon the as-synthesized Pt catalysts and Pt-free Silicalite-1, measured at the reaction temperature of 353 K and space velocity of 1.1×10^6 mL g_{cat}⁻¹ h⁻¹ with 80% H₂–Ar and liquid 20 wt % HDO–H₂O as feeds, and (b) Arrhenius plots of gas-phase deuterium extraction rate upon these Pt catalysts at the feeding of 70 kPa H₂, 10 kPa vapor (20% HDO in H₂O), and balanced Ar at the space velocity of 5×10^6 mL g_{cat}⁻¹ h⁻¹.

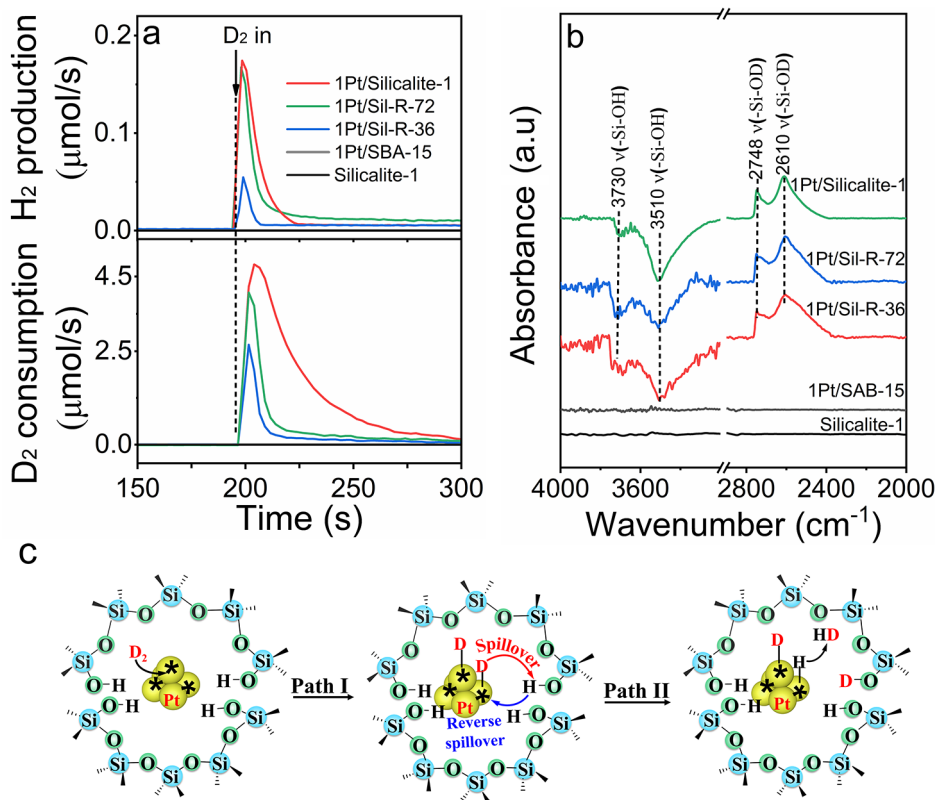


Figure 5. (a) TSR spectra of D₂ adsorption on prerduced Pt catalysts and Pt-free Silicalite-1 at 353 K by tracing H₂ ($m/z = 2$) and D₂ ($m/z = 4$) signals and quantifying with internal standard gas. (b) FT-IR absorption spectra taken after 1 kPa of D₂ adsorption at 353 K on these Pt samples and Silicalite-1 by using the annealed samples as background and (c) schematic of the proposed pathway for deuterium spillover and hydrogen reverse spillover during D₂ adsorption.

with the catalytic activities being undetectable due to the lack of active metal sites. Figure 4a shows the deuterium extraction rate during H₂–HDO isotope exchange on the as-synthesized Pt catalysts at the constant space velocity of 1.1×10^6 mL g_{cat}⁻¹ h⁻¹. At a glance, the the 1Pt/Silicalite-1 catalyst exhibits the superior deuterium extraction reactivity at 353 K, whose rate is nearly 10 times higher than that of 1Pt/SBA-15. When

crystallizing the amorphous SBA-15 framework under hydrothermal conditions for 72 h, the deuterium extraction rate of the 1Pt/Sil-R-72 catalyst is accelerated by 7 times due to the formation of zeolitic framework. Further, the intrinsic reactivities of H₂–HDO exchange upon these supported Pt catalysts were measured in the kinetically controlled regime at the gas-phase reaction condition by the extensive intrapellet

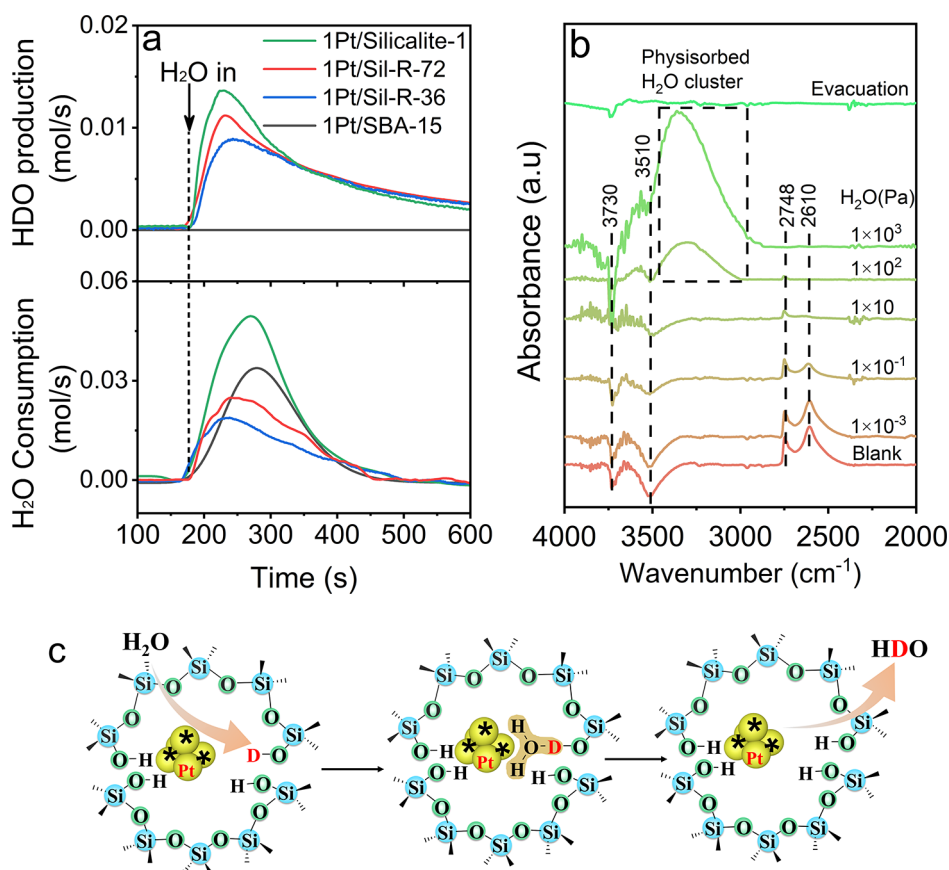


Figure 6. (a) TSR spectra of H₂O adsorption on the deuterated Pt catalysts at 353 K by tracing H₂O ($m/z = 18$) and HDO ($m/z = 19$) signals. (b) FT-IR absorption spectra, taken during H₂O adsorption on 1Pt/Silicalite-1 at the different partial pressures by using the annealed samples as background. (c) Schematic of the proposed pathway for hydrogen–deuterium exchange on the deuterated 1Pt/Silicalite-1 sample during H₂O adsorption.

dilution to eliminate the kinetic artifact from mass transfer limitation. H₂–HDO reactions on these Pt catalysts (1Pt/Silicalite-1, 1Pt/SBA-15, and 1Pt/Sil-R- x) at the gas-phase condition of 70 kPa H₂ and 10 kPa HDO–H₂O vapor reached the steady-state above 0.5 h, and the deuterium extraction rates varied by less than 10% of the measured values. Figure 4b shows the deuterium extraction rates on these Pt catalysts, plotted as a function of the inverse temperature in the Arrhenius form. Upon the series of Pt catalysts, although their particle size and active site densities remain similar, the measured deuterium extraction rate in the temperature range of 323–353 K increases by this order: 1Pt/SBA-15 < 1Pt/Sil-R-36 < 1Pt/Sil-R-72 < 1Pt/Silicalite-1. Correspondingly, the apparent activation energy (E_a , shown in Table 1) decreases from 49.2 kJ mol⁻¹ for 1Pt/SBA-15 to 36.9 kJ mol⁻¹ for 1Pt/Silicalite-1. In our previous studies,³⁹ the deuterium extraction rates upon Pt/ZSM-5 during H₂–HDO isotope exchange are closely related to their Pt particle size and BA concentration, while the catalytic contributions in the current as-used catalysts from the differently exposed Pt atoms and protonic sites could be completely excluded because of the resemble Pt cluster size and ignorable BA. Such an increase in reaction rate and decrease in activation barrier might be associated with the formation of unique reactive sites on the siliceous zeolite framework, which is highly efficient to catalyze hydrogen isotope exchange. Next, we interrogate the active structures of Pt supported on the zeolitic silica, specifically, the nature of

active sites and its catalytic role that leads to the exceptionally high reaction rate.

3.3. Exploring the Reaction Pathway of Hydrogen and Water on the As-Synthesized Pt Catalysts by In Situ Spectroscopy and Density Functional Theory. To ascertain the reactive sites formed on these Pt catalysts for isotope exchange, transient surface reaction (TSR) and in situ FT-IR were employed to interrogate the surface chemistry of hydrogen and water. For these hydrogen-type Pt samples, the hydrogen of hydroxyls within their frameworks is very difficult to completely exchange by deuterium via the hydrothermal treatment with D₂O, leading to the coexistence of hydroxyl and deuterioxyl groups on the siliceous framework. To acquire the intensive signals and exclude possible interference from hydrogen isotopes during spectroscopic experiments, D₂ and H₂O were considered as the probe molecules to study the surface adsorption and reaction. As shown in Figure 5a, when exposing the purified D₂ ($m/z = 4$) to these zeolitic Pt catalysts (e.g., 1Pt/Silicalite-1 and 1Pt/Sil-R- x) at 353 K, the H₂ ($m/z = 2$) and HD ($m/z = 3$ in Figure S4a) signals in the effluent are monitored by an online mass spectrometer (MS), while the H₂ and HD formation and D₂ consumption on 1Pt/SBA-15 and Pt-free Silicalite-1 are not observed during the entire stage. Noticeably, H₂ production rate synchronously varies with D₂ ($m/z = 4$) consumption and the accumulative hydrogen production in Figure S4b is comparable to the deuterium consumption. These correlations suggest that the siliceous zeolite framework possesses highly reactive sites to react with

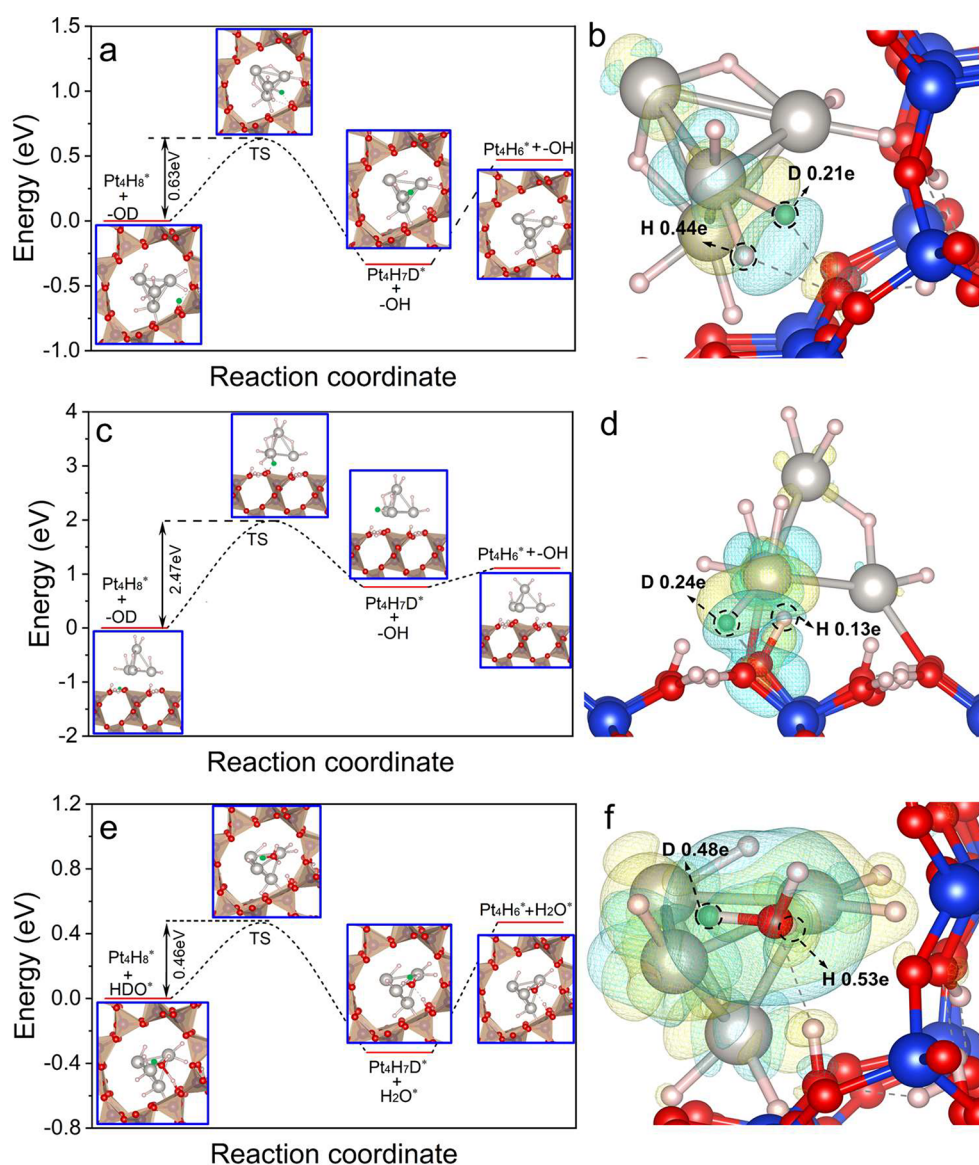


Figure 7. Reaction pathways of hydrogen transfer upon (a) Pt/Silicalite-1, (c) Pt/SBA-15, and (e) HDO covered Pt/Silicalite-1. The corresponding charge density differences between the transition state and initial state for hydrogen transfer are shown for (b) Pt/Silicalite-1, (d) Pt/SBA-15, and (f) HDO covered Pt/Silicalite-1. The yellow and cyan clouds represent charge accumulation and depletion, respectively. Pt, Si, H, O, and D atoms are shown in gray, blue, pink, red, and green, respectively. The structural configurations of reactive sites are locally magnified, and the intact structural models are shown in Figure S7.

the dissociated deuterium on Pt clusters by isotope exchange. To systematically understand the reaction chemistry during D₂ feeding, in situ FT-IR spectra in Figure 5b show that the exposure of 1 kPa D₂ to the hydrogen-reduced 1Pt/Silicalite-1 and 1Pt/Sil-R-*x* catalysts at 353 K causes two characteristic peaks which emerged at 2748 and 2610 cm⁻¹, corresponding to the weak hydrogen-bonded deuterated silanols (-Si-OD-O-) and the strong hydrogen-bonded deuterated silanols (-Si-OD-O-Si-) upon the zeolite framework,^{30,40} respectively, while the isotopically exchanged deuteroyls are not observed on 1Pt/SBA-15 because of the extremely weak acidity of its isolated silanols with pK_a values of 5.94–11.24 enabling the hydrogen as a proton donor to be improbable.⁴¹ The formation of deuterated silanols on 1Pt/Silicalite-1 and 1Pt/Sil-R-*x* is due to the hydrogen-bonded silanols donating their hydrogen atoms and participating in the surface reaction in the form of protons,³⁰ which involves the hydrogen transfer from

silanols within the zeolite framework to Pt sites and the spill-back of dissociated deuterium from Pt to the defective oxygen site to generate the deuterated silanols, as depicted by Path I in Figure 5c. After completing the H–D exchange, the reverse spilt-over hydrogen on Pt sites combines with each other or the other deuterium to desorb in the form of H₂ or HD, contributing to the observed products during the TSR experiment. The substitution of hydrogen for silanols by deuterium enables the hydroxyl stretching to be perturbed, leading to the corresponding negative peaks formed at 3730 and 3510 cm⁻¹ when using the sample as background. The presence of H–D exchange upon these zeolitic Pt catalysts demonstrates that these hydrogen-bonded silanols within the zeolite framework serve as the reactive sites of H₂–HDO isotope exchange.

After isotopically exchanging the hydrogen of silanols on the as-synthesized Pt catalysts by D₂ exposure, H₂O (*m/z* = 18)

vapor is fed to contact with these samples for surface reaction. In the TSR spectra in Figure 6a, H₂O ($m/z = 18$) adsorption upon these deuterated 1Pt/Silicalite-1 and 1Pt/Sil-R-*x* catalysts causes HDO ($m/z = 19$) to be produced in the effluent due to the surface reaction of H₂O and deuterioxy. On the 1Pt/SBA-15 sample, no HDO signal is observed and H₂O uptake in mesoporous channels causes the consumption rate to increase firstly and then decrease with stream-on-time. To ensure the reactive sites of H₂O upon these deuterated Pt catalysts, a trace amount of purified H₂O vapor was exposed to the wafer at 353 K under a dynamic vacuum for the spectroscopic analysis by in situ FT-IR. In Figure 6b, it is found that H₂O predominantly adsorbs on the deuterated silanols of 1Pt/Silicalite-1 and undergoes a rapid isotope exchange by forming the positively charged H₂DO intermediate and then desorbing in the form of HDO, as depicted in Figure 6c, causing the simultaneous attenuation of absorption bands at 2748 and 2610 cm⁻¹ and the recovery of negative peaks at 3730 and 3510 cm⁻¹ with H₂O feeding. When increasing H₂O partial pressure to ~100 Pa, the excessive H₂O adsorption on these hydrogen-bonded silanols of Silicalite-1 enables the characteristic peaks at 3730 and 3510 cm⁻¹ to become more negative, accompanied by the appearance of a broad band at 3354 cm⁻¹ due to the formation of hydrogen-bonded water clusters.³³ After the vigorous evacuation, the adsorbed water clusters were removed completely, leading to the re-recovery of negative peaks. Similarly, the successive H₂O adsorption on the deuterated 1Pt/Sil-R-36 and 1Pt/Sil-R-72 catalysts in Figure S5 also experience the above-described process with the isotope exchange at the initial stage and the secondary adsorption on the new sites at the later stage. For the 1Pt/SBA-15 catalyst with the isolated silanols at 3745 cm⁻¹ in Figure S6, D₂O adsorption at the identical experiment condition causes the emergence of deuterated silanols at 2758 cm⁻¹ and the formation of a negative peak at 3745 cm⁻¹, which suggests that the silanols contained within the amorphous framework of SBA-15 are highly reactive to the H–D exchange caused by water adsorption but inert to the isotope exchange driven by the hydrogen transfer between metal and supports.

The reaction pathways of hydrogen isotope exchange on the acidic Pt–zeolite catalysts primarily involve the activation of water clusters on protonic sites to deliver deuterons and the positively charged hydrogen/deuterium transfer between Pt and zeolite to attain H–D exchange, during which the reverse spillover of deuterium functions as the kinetic-relevant steps.³⁹ In this case, it is found that water adsorption on the silanols contained within the siliceous frameworks of 1Pt/Silicalite-1 and 1Pt/SBA-15 is energetically favorable, with the apparent hydroxyl/deuterioxy exchange during the FT-IR experiment. Consequently, the kinetically relevant hydrogen transfer step was further interrogated by density functional theory (DFT) calculations to address the underlying mechanisms. The reactive sites in Silicalite-1 were constructed by creating four defective sites in the orthorhombic cell of MFI unit with the dangling bonds saturated by hydrogen atoms to represent the hydrogen-bonded silanols. For comparison, the amorphous framework in SBA-15 was modeled by extracting the (100) surface of bulk α -quartz with four layers, containing silanols populated on the surface. As shown in Figure 7a, the dissociated H on the Pt₄ cluster can approach the oxygen atom of deuterioxy within the zeolite framework under the electrostatic attraction interaction, and simultaneously the D

atom of deuterioxy scrambles to the Pt site by a transition state with an energy barrier of 0.63 eV, leading to the prolonged Pt–H and O–D bond lengths of 1.611 and 1.690 Å (relative to the original values of 1.550 and 0.983 Å), respectively. In contrast, the resembled H and D transfer at the interface of Pt and SBA-15 requires an energy barrier of 2.47 eV in Figure 7c, which is much larger than that on Pt/Silicalite-1. This implies the energetically improbable hydrogen transfer upon the Pt/SBA-15 sample, coinciding with the spectroscopic observation by TSR and FT-IR experiments. To understand the charge transfer during the H/D atom mobility, the charge density differences for the structural configuration at the transition state on Pt/Silicalite-1 and Pt/SBA-15 are shown in Figures 7b and 7d, respectively. It can be seen that the electron accumulation primarily occurs on the Pt that neighbored the D atom and the electron depletion on the original O–D bond. Thus, the charges transfer from deuterioxy to Pt, which greatly weakens the original O–D bond and promotes the formation of a Pt–D bond. However, the remarkable energy barrier difference between Pt/Silicalite-1 and Pt/SBA-15 might arise from the distinct charge states of active atoms. The Bader charges of D atoms for the reverse spillover on these samples are comparable mutually, varied in the range of 0.21–0.24 e. But the charge of H atoms for the spillover on Pt/Silicalite-1 is 0.44 e, much higher than that of 0.24 e on Pt/SBA-15. Thus, the hydrogen spillover on Pt/SBA-15 requires more charge transfers and the adsorbed hydrogen tends to dwell on the Pt site rather than the O atom of silanol, leading to the higher activation energy barrier to cleave the O–D bond. Indeed, the liquid phase H₂–HDO reaction upon these Pt catalysts enables the reactive silanols to be predominantly covered by water due to the high affinity.⁴² To elucidate the role of water during hydrogen transfer, an HDO molecule was placed on the silanol site to model the authentic reaction environment. Within the siliceous zeolite framework, water easily adsorbs on the hydroxyl site by the hydrogen bond with the ignorable activation energy.⁴³ As shown in Figure 7e, the D atom of hydrogen-bonded HDO and the adsorbed H on Pt sites undergo a bidirectional migration, similar to the above-described process to attain H–D exchange between Pt and the hydrogen-bonded water. Benefiting from the water-mediated interaction, the energy barrier for this migration is 0.46 eV and the Bader charges of D and H atoms in Figure 7f are 0.48 and 0.53 e, respectively. The less charge transfer and the lower energy barrier suggest that the hydrogen transfer upon Pt/Silicalite-1 preferentially proceeds by the water-assisted hydrogen spillover and deuterium reverse spillover. After completing the interfacial H–D exchange, the adsorbed D on Pt can easily combine with the other H atom to desorb in the form of HD.

4. CONCLUSION

A series of supported Pt catalysts with tunable silica frameworks were prepared to interrogate the hydrogen transfer between metal and supports and its promotional effect to the liquid phase H₂–HDO isotope exchange. The formation of crystallized zeolite frameworks enables the hydrogen transfer between Pt and inert silica to become possible, leading to the deuterium extraction rate during the H₂–HDO reaction being 10 times higher than that on traditional Pt/SBA-15 at the optimum condition. On this basis, in situ spectroscopic and theoretical studies suggest that the defective silanols formed within the zeolite framework serve as the reactive site to attain

the interfacial hydrogen transfer. This process substantially involves two primary reaction steps: (1) water adsorbs on these sites to form the hydrogen-bonded intermediate and (2) the hydrogen adsorbed on Pt sites and the deuterium of bonded water experience a simultaneous and bidirectional migration with the electrostatic attraction interaction to attain H–D exchange in the positively charged form. Ultimately, the reverse spilt-over deuterium on Pt combines with the other hydrogen on Pt to desorb, contributing to the HD product. These findings uncover the nature of hydrogen transfer between metal and nonreducible silica and favor the development of highly efficient metal catalysts for hydrogen–water isotope exchange and other hydrogen-involving reactions.

■ ASSOCIATED CONTENT

Data Availability Statement

Data will be made available on request.

Supporting Information

The Supporting Information is available free of charge at <https://pubs.acs.org/doi/10.1021/acsami.4c03725>.

N₂ adsorption/desorption isotherms and pore size distribution of the as-synthesized Pt-based catalysts; XPS Pt 4f spectra and contact angle of droplets on the smooth surface of different catalysts; TSR spectra of D₂ adsorption on the prerduced Pt-based catalyst samples at 353 K; in situ FT-IR absorption spectra of H₂O/D₂O adsorption; and atomistic structures for hydrogen transfer on Pt/Silicalite-1 and Pt/SBA-15 (PDF)

■ AUTHOR INFORMATION

Corresponding Authors

Yifei Yang – Institute of Materials, China Academy of Engineering Physics, Jianguyou 621908, China; orcid.org/0000-0002-3674-4488; Email: yangyifei@caep.cn

Shutao Xu – National Engineering Research Center of Lower-Carbon Catalysis Technology, Dalian Institute of Chemical Physics, Chinese Academy of Sciences, Dalian 116023, China; orcid.org/0000-0003-4722-8371; Email: xushutao@dicp.ac.cn

Yunxi Yao – Institute of Materials, China Academy of Engineering Physics, Jianguyou 621908, China; orcid.org/0000-0002-0814-6675; Email: yaoyunxi@caep.cn

Authors

Hongbing Wang – Institute of Materials, China Academy of Engineering Physics, Jianguyou 621908, China; orcid.org/0000-0002-1952-415X

Yida Zhou – National Engineering Research Center of Lower-Carbon Catalysis Technology, Dalian Institute of Chemical Physics, Chinese Academy of Sciences, Dalian 116023, China

Jun Chen – Institute of Materials, China Academy of Engineering Physics, Jianguyou 621908, China

Dongping Wang – Institute of Materials, China Academy of Engineering Physics, Jianguyou 621908, China

Wei Cui – School of Chemical Sciences, University of Chinese Academy of Sciences, Beijing 100049, China

Linsen Zhou – Institute of Materials, China Academy of Engineering Physics, Jianguyou 621908, China; orcid.org/0000-0001-7408-9720

Complete contact information is available at: <https://pubs.acs.org/doi/10.1021/acsami.4c03725>

Author Contributions

H.W.: data curation, investigation, writing—original draft. Y.Y.: conceptualization, investigation, formal analysis, writing—review and editing. Y.Z.: investigation. J.C.: investigation. D.W.: investigation. W.C.: investigation. L.Z.: investigation. S.X.: investigation. Y.Y.: conceptualization, writing—review and editing.

Notes

The authors declare no competing financial interest.

■ ACKNOWLEDGMENTS

This work was financially supported by the National Natural Science Foundation of China (NSFC) (22002144, 22109147, and 22241801).

■ REFERENCES

- (1) Li, Z.; Ren, Q.; Wang, X.; Chen, W.; Leng, L.; Zhang, M.; Horton, J. H.; Liu, B.; Xu, Q.; Wu, W.; Wang, J. Highly Active and Stable Palladium Single-Atom Catalyst Achieved by a Thermal Atomization Strategy on an SBA-15 Molecular Sieve for Semi-Hydrogenation Reactions. *ACS Appl. Mater. Interfaces* **2021**, *13* (2), 2530–2537.
- (2) Perumal, S. K.; Lee, S.; Yu, H.; Heo, J.; Kang, M. J.; Kim, Y.; Park, M.; Lee, H.; Kim, H. S. Synergistic Interaction between Ruthenium Catalysts and Grafted Niobium on SBA-15 for 2,5-Furandicarboxylic Acid Production Using 5-Hydroxymethylfurfural. *ACS Appl. Mater. Interfaces* **2024**, *16* (6), 7353–7363.
- (3) Liang, J.; Liang, Z.; Zou, R.; Zhao, Y. Heterogeneous Catalysis in Zeolites, Mesoporous Silica, and Metal–Organic Frameworks. *Adv. Mater.* **2017**, *29* (30), 1701139.
- (4) Miller, J. T.; Pei, S. Hydrogenation and deuterium exchange by spillover hydrogen of ethylbenzene adsorbed on H-USY zeolite. *Appl. Catal., A* **1998**, *168* (1), 1–7.
- (5) Tan, Y.; Han, M.; Peng, P.; Sun, Z.; Shi, J.; Huang, Y.; Chen, J.; Bai, L.; Yang, J.; Chen, Q. Strengthening spillover hydrogenation of quinoline compounds over platinum-encapsulated amorphized HA zeolite catalyst. *Mol. Catal.* **2023**, *545*, 113210.
- (6) Im, J.; Shin, H.; Jang, H.; Kim, H.; Choi, M. Maximizing the catalytic function of hydrogen spillover in platinum-encapsulated aluminosilicates with controlled nanostructures. *Nat. Commun.* **2014**, *5*, 3370.
- (7) Shun, K.; Mori, K.; Masuda, S.; Hashimoto, N.; Hinuma, Y.; Kobayashi, H.; Yamashita, H. Revealing hydrogen spillover pathways in reducible metal oxides. *Chem. Sci.* **2022**, *13* (27), 8137–8147.
- (8) Prins, R. Hydrogen spillover. Facts and fiction. *Chem. Rev.* **2012**, *112* (5), 2714–38.
- (9) Triwahyono, S.; Jalil, A. A.; Timmiati, S. N.; Ruslan, N. N.; Hattori, H. Kinetics study of hydrogen adsorption over Pt/MoO₃. *Appl. Catal., A* **2010**, *372* (1), 103–107.
- (10) Prins, R.; Palfi, V. K.; Reiher, M. Hydrogen Spillover to Nonreducible Supports. *J. Phys. Chem. C* **2012**, *116* (27), 14274–14283.
- (11) Shen, H.; Li, H.; Yang, Z.; Li, C. Magic of hydrogen spillover: Understanding and application. *Green Energy Environ.* **2022**, *7* (6), 1161–1198.
- (12) Xing, S.; Xiong, M.; Zhao, S.; Zhang, B.; Qin, Y.; Gao, Z. Improving the Efficiency of Hydrogen Spillover by an Organic Molecular Decoration Strategy for Enhanced Catalytic Hydrogenation Performance. *ACS Catal.* **2023**, *13* (6), 4003–4011.
- (13) Tan, M.; Yang, Y.; Yang, Y.; Chen, J.; Zhang, Z.; Fu, G.; Lin, J.; Wan, S.; Wang, S.; Wang, Y. Hydrogen spillover assisted by oxygenate molecules over nonreducible oxides. *Nat. Commun.* **2022**, *13* (1), 1457.
- (14) Stolle, S.; Sümmchen, L.; Roland, U.; Herzog, K.; Salzer, R. Application of FTIR microscopy for the investigation of the H–D exchange on Y zeolites - deuterium spillover as reaction pathway. *J. Mol. Struct.* **1995**, *349*, 93–96.

- (15) Schuetze, F. W.; Roessner, F.; Meusinger, J.; Papp, H. Hydrogen/deuterium exchange on dealuminated H-ZSM-5 zeolites studied by time resolved FTIR spectroscopy. *Stud. Surf. Sci. Catal.* **1997**, *112*, 127–134.
- (16) Shin, H.; Choi, M.; Kim, H. A mechanistic model for hydrogen activation, spillover, and its chemical reaction in a zeolite-encapsulated Pt catalyst. *Phys. Chem. Chem. Phys.* **2016**, *18* (10), 7035–41.
- (17) Luo, Y.; Miao, C.; Yue, Y.; Hua, W.; Gao, Z. ZnO supported on Silicalite-1 as an efficient catalyst for isobutane dehydrogenation to isobutene assisted by CO₂. *Microporous Mesoporous Mater.* **2020**, *294*, 109864.
- (18) Wu, L.; Ren, Z.; He, Y.; Yang, M.; Yu, Y.; Liu, Y.; Tan, L.; Tang, Y. Atomically Dispersed Co²⁺ Sites Incorporated into a Silicalite-1 Zeolite Framework as a High-Performance and Coking-Resistant Catalyst for Propane Nonoxidative Dehydrogenation to Propylene. *ACS Appl. Mater. Interfaces* **2021**, *13* (41), 48934–48948.
- (19) Cheng, Y.; Lei, T.; Miao, C.; Hua, W.; Yue, Y.; Gao, Z. Single-Site CrOx Moieties on Silicalite: Highly Active and Stable for Ethane Dehydrogenation with CO₂. *Catal. Lett.* **2018**, *148* (5), 1375–1382.
- (20) Kubota, S.; Sumi, T.; Kitamura, H.; Miyake, K.; Uchida, Y.; Nishiyama, N. Promoted propane dehydrogenation over Co confined within core-shell silicalite-1 zeolite crystals. *Catal. Sci. Technol.* **2024**, *14*, 1201–1208.
- (21) Xu, Y.; Xin, F.; Jiang, Y.; Yin, X. Liquid-Phase Catalytic Exchange of Hydrogen Isotopes over Platinum on Dual-Modified Graphene. *ACS Appl. Mater. Interfaces* **2021**, *13* (27), 31660–31667.
- (22) Fu, X.; Hou, J.; Chen, C.; Li, J.; Yue, L.; Chen, X.; Zhao, L.; Ran, G.; Xia, X.; Gong, Y.; Ding, W.; Xiao, C.; Wang, H. Superhydrophobic and superaerophilic hierarchical Pt@MIL-101/PVDF composite for hydrogen water isotope exchange reactions. *J. Hazard. Mater.* **2019**, *380*, 120904.
- (23) Marcus, G. H. Nuclear power around the world. *Nat. Rev. Phys.* **2019**, *1* (3), 172–173.
- (24) Lin, L.; Zhou, W.; Gao, R.; Yao, S.; Zhang, X.; Xu, W.; Zheng, S.; Jiang, Z.; Yu, Q.; Li, Y.-W.; Shi, C.; Wen, X.-D.; Ma, D. Low-Temperature Hydrogen Production from Water and Methanol using Pt/ α -MoC Catalysts. *Nature* **2017**, *544*, 80–83.
- (25) Liu, L.; Lopez-Haro, M.; Lopes, C. W.; Li, C.; Concepcion, P.; Simonelli, L.; Calvino, J. J.; Corra, A. Regioselective generation and reactivity control of subnanometric platinum clusters in zeolites for high-temperature catalysis. *Nat. Mater.* **2019**, *18* (8), 866–873.
- (26) Emeis, C. A. Determination of Integrated Molar Extinction Coefficients for Infrared Absorption Bands of Pyridine Adsorbed on Solid Acid Catalysts. *J. Catal.* **1993**, *141* (2), 347–354.
- (27) Kim, K. C.; Moschetta, E. G.; Jones, C. W.; Jang, S. S. Molecular Dynamics Simulations of Aldol Condensation Catalyzed by Alkylamine-Functionalized Crystalline Silica Surfaces. *J. Am. Chem. Soc.* **2016**, *138* (24), 7664–7672.
- (28) Liang, H.; Zhang, B.; Gao, P.; Yu, X.; Liu, X.; Yang, X.; Wu, H.; Zhai, L.; Zhao, S.; Wang, G.; van Bavel, A. P.; Qin, Y. Strong Co-O-Si bonded ultra-stable single-atom Co/SBA-15 catalyst for selective hydrogenation of CO₂ to CO. *Chem. Catal.* **2022**, *2* (3), 610–621.
- (29) Reichinger, M.; Schmidt, W.; Narkhede, V. V.; Zhang, W.; Gies, H.; Grünert, W. Ordered mesoporous materials with MFI structured microporous walls – Synthesis and proof of wall microporosity. *Microporous Mesoporous Mater.* **2012**, *164*, 21–31.
- (30) Dib, E.; Costa, I. M.; Vayssilov, G. N.; Aleksandrov, H. A.; Mintova, S. Complex H-bonded silanol network in zeolites revealed by IR and NMR spectroscopy combined with DFT calculations. *J. Mater. Chem. A* **2021**, *9* (48), 27347–27352.
- (31) Liu, Y.; Liu, Z.; Hui, Y.; Wang, L.; Zhang, J.; Yi, X.; Chen, W.; Wang, C.; Wang, H.; Qin, Y.; Song, L.; Zheng, A.; Xiao, F.-S. Rhodium nanoparticles supported on silanol-rich zeolites beyond the homogeneous Wilkinson's catalyst for hydroformylation of olefins. *Nat. Commun.* **2023**, *14* (1), 2531.
- (32) Wu, Z.; Zhang, C.; Peng, L.; Wang, X.; Kong, Q.; Gu, X. Enhanced Stability of MFI Zeolite Membranes for Separation of Ethanol/Water by Eliminating Surface Si–OH Groups. *ACS Appl. Mater. Interfaces* **2018**, *10* (4), 3175–3180.
- (33) Li, G.; Wang, B.; Kobayashi, T.; Pruski, M.; Resasco, D. E. Optimizing the surface distribution of acid sites for cooperative catalysis in condensation reactions promoted by water. *Chem. Catal.* **2021**, *1* (5), 1065–1087.
- (34) Liu, C.; Zhu, P.; Wang, J.; Liu, H.; Zhang, X. Geometrically embedding dispersive Pt nanoparticles within silicalite-1 framework for highly selective α , β -unsaturated aldehydes hydrogenation via oriented C = O adsorption configuration. *Chem. Eng. J.* **2022**, *446*, 137064.
- (35) Bocus, M.; Goeminne, R.; Lataire, A.; Cools-Ceuppens, M.; Verstraelen, T.; Van Speybroeck, V. Nuclear quantum effects on zeolite proton hopping kinetics explored with machine learning potentials and path integral molecular dynamics. *Nat. Commun.* **2023**, *14* (1), 1008.
- (36) Sun, Q.; Gao, H.; Sema, T.; Liang, Z. Enhanced CO₂ desorption rate for rich amine solution regeneration over hierarchical HZSM-5 catalyst. *Chem. Eng. J.* **2023**, *469*, 143871.
- (37) Ravi, M.; Sushkevich, V. L.; van Bokhoven, J. A. On the location of Lewis acidic aluminum in zeolite mordenite and the role of framework-associated aluminum in mediating the switch between Brønsted and Lewis acidity. *Chem. Sci.* **2021**, *12* (11), 4094–4103.
- (38) Padovan, D.; Al-Nayili, A.; Hammond, C. Bifunctional Lewis and Brønsted acidic zeolites permit the continuous production of bio-renewable furanic ethers. *Green Chem.* **2017**, *19* (12), 2846–2854.
- (39) Wang, H.; Yang, Y.; Yu, S.; Zhang, B.; Xie, J.; Chen, J.; Wang, D.; Feng, B.; Zhong, C.; Zhou, L.; Cui, W.; Ma, D.; Yao, Y. Insight into the hydrogen mobility upon Pt/ZSM-5 and its catalytic function during liquid-phase hydrogen isotopes exchange. *J. Catal.* **2024**, *430*, 115345.
- (40) Karbowski, T.; Saada, M.-A.; Rigolet, S.; Ballandras, A.; Weber, G.; Bezverkhyy, I.; Soulard, M.; Patarin, J.; Bellat, J.-P. New insights in the formation of silanol defects in silicalite-1 by water intrusion under high pressure. *Phys. Chem. Chem. Phys.* **2010**, *12* (37), 11454–11466.
- (41) Liu, D.; Ma, G.; Allen, H. C. Adsorption of 4-Picoline and Piperidine to the Hydrated SiO₂ Surface: Probing the Surface Acidity with Vibrational Sum Frequency Generation Spectroscopy. *Environ. Sci. Technol.* **2005**, *39* (7), 2025–2032.
- (42) Gallas, J.-P.; Goupil, J.-M.; Vimont, A.; Lavalley, J.-C.; Gil, B.; Gilson, J.-P.; Miserque, O. Quantification of Water and Silanol Species on Various Silicas by Coupling IR Spectroscopy and in-Situ Thermogravimetry. *Langmuir* **2009**, *25* (10), 5825–5834.
- (43) Treps, L.; Gomez, A.; de Bruin, T.; Chizallet, C. Environment, Stability and Acidity of External Surface Sites of Silicalite-1 and ZSM-5 Micro and Nano Slabs, Sheets, and Crystals. *ACS Catal.* **2020**, *10* (5), 3297–3312.